Science of the Total Environment 854 (2023) 158774

Contents lists available at ScienceDirect

Science of the Total Environment

journal homepage: www.elsevier.com/locate/scitotenv

A molecular study of Italian ryegrass grown on Martian regolith simulant

Roberto Berni [a], Céline C. Leclercq [a], Philippe Roux [b], Jean-Francois Hausman [a], Jenny Renaut [a], Gea Guerriero [a,*]

[a] Luxembourg Institute of Science and Technology (LIST), Environmental Research and Innovation (ERIN) Department, L-4940 Hautcharage, Luxembourg
[b] Gembloux Agro-Bio Tech, TERRA Teaching and Research Centre, University of Liège, B-5030 Gembloux, Belgium

HIGHLIGHTS

- Italian ryegrass grew on Martian regolith simulants MMS-1
- Plants on MMS-1 showed chlorotic leaves and developed root aerenchyma
- Genes involved in stress response/primary metabolism changed in expression on MMS-1
- Proteins involved in translation and DNA methylation changed in abundance on MMS-1
- Plants significantly modified the pH of MMS-1 over a time of 2 weeks

GRAPHICAL ABSTRACT

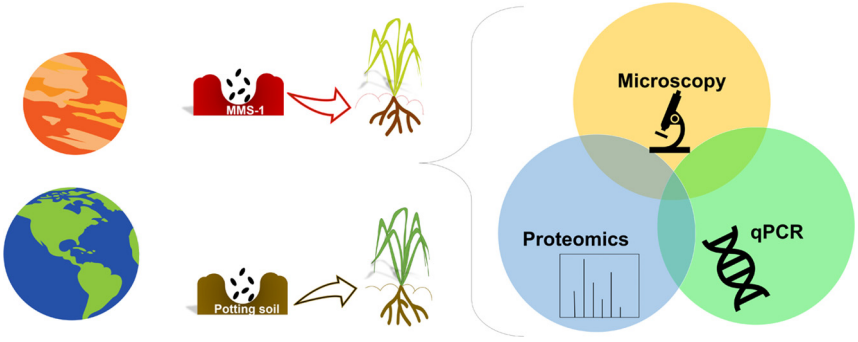

ARTICLE INFO

Editor: Charlotte Poschenrieder

Keywords:
Martian regolith simulants
In situ resource utilization
Lolium multiflorum
Microscopy
qPCR
Proteomics

ABSTRACT

In the last decade, the exploration of deep space has become the objective of the national space programs of many countries. The International Space Exploration Coordination Group has set a roadmap whose long-range strategy envisions the expansion of human presence in the solar system to progress with exploration and knowledge and to accelerate innovation. Crewed missions to Mars could be envisaged by 2040. In this scenario, finding ways to use the local resources for the provision of food, construction materials, propellants, pharmaceuticals is needed. Plants are important resources for deep space manned missions because they produce phytochemicals of pharmaceutical relevance, are sources of food and provide oxygen which is crucial in bioregenerative life support systems. Growth analysis and plant biomass yield have been previously evaluated on Martian regolith simulants; however, molecular approaches employing gene expression analysis and proteomics are still missing. The present work aims at filling this gap by providing molecular data on a representative member of the Poaceae, *Lolium multiflorum* Lam., grown on potting soil and a Martian regolith simulant (MMS-1). The molecular data were complemented with optical microscopy of root/leaf tissues and physico-chemical analyses. The results show that the plants grew for 2 weeks on regolith simulants. The leaves were bent downwards and chlorotic, the roots developed a lacunar aerenchyma and small brownish deposits containing Fe were observed. Gene expression analysis and proteomics revealed changes in transcripts related to the phenylpropanoid pathway, stress response, primary metabolism and proteins involved in translation and DNA methylation. Additionally, the growth of plants slightly but significantly modified the pH of the regolith simulants. The results here presented constitute a useful resource to get a comprehensive understanding of the major factors impacting the growth of plants on MMS-1.

1. Introduction

The Global Exploration Roadmap (Hufenbach et al., 2011) established by the International Space Exploration Coordination Group (ISECG) envisions long-term spaceflight missions that go far beyond low Earth orbit (LEO). The Moon, together with the cis-lunar space, Near-Earth Asteroids

* Corresponding author.
E-mail address: gea.guerriero@list.lu (G. Guerriero).

http://dx.doi.org/10.1016/j.scitotenv.2022.158774
Received 8 July 2022; Received in revised form 10 September 2022; Accepted 10 September 2022
Available online 13 September 2022

and the Mars system are the destinations considered in the long-range strategy to extend human presence in space (Hufenbach et al., 2011). In this context, it is evident that the cost, technical challenges and risks associated with the supply of resources from Earth constitute important limitations for space exploration. Hence, *in situ* resource utilization (ISRU), i.e., the use of raw materials derived locally, solves these issues by offering *in loco* what is needed to support human space exploration (Berliner et al., 2021; Menezes et al., 2015). For instance, some authors suggested that raw materials to manufacture structures and equipment may be obtained by extracting minerals and metals from regoliths via reduction processes (Meurisse and Carpenter, 2020). Glass substrates and sintered ceramics can be obtained by processing Moon and Martian regoliths, respectively (Karl et al., 2020; Schleppi et al., 2019). Compressed regoliths display significant thermal insulation, protect from the radiations and are therefore useful construction materials for the establishment of future colonies (Akisheva and Gourinat, 2021).

The future human presence on Moon or Mars will also rely on crops produced on board spacecraft during long-term space missions and *in situ* as source of food, oxygen and bioactive compounds, such as antioxidants with health-promoting properties (Duri et al., 2020; Salisbury, 1999).

In the context of deep space exploration, one of the most important challenges is to produce food *in situ* as an alternative to cargo shipments from Earth (Wamelink et al., 2014). Even if the presence of water on the Martian and Lunar surface (Hui et al., 2013; Möhlmann, 2004) could be used for hydroponic and aeroponic cultivations, the most practical solution is to use the native regoliths for plant growth. This option allows indeed to fly only the seeds besides the equipment, such as lamps (Wamelink et al., 2019).

Growing edible plants on board spacecrafts and *in situ* on Martian or Lunar surfaces allows an adequate CO_2/O_2 balance for sustaining life (De Micco et al., 2009; Lasseur et al., 2010), while producing food for deep space travellers and the future colonists. Furthermore, the water transpired and purified by plants can be condensed and recycled to contribute to the system's water cycle (Pickett et al., 2020).

Extra-terrestrial regolith-sampling robots on landers/rovers have collected samples (Qian et al., 2021; Zhang et al., 2019), making it possible to study Lunar and Martian regoliths (Grotzinger et al., 2012) and develop simulants (Allen et al., 1998; Cannon et al., 2019; Peters et al., 2008; Ramkissoon et al., 2019). Recently, the available Lunar and Martian regolith simulants were comprehensively reviewed based on their properties (Duri et al., 2022); of the available ones, 3 Martian regolith simulants are commercialized, i.e., JEZ-1 Jezero Delta Simulant, MGS-1 Mars Global Simulant, MGS-1C and MGS-1S (Clay/Sulfate ISRU) (Cannon et al., 2019 and available from https://exolithsimulants.com/products/jez-1-jezero-delta-simulant), as well as MMS-1/2 Mojave Mars Simulant, Enhanced Mars Simulant (Caporale et al., 2020 and available from https://www.themartiangarden.com/). Simulants help test fundamental questions, such as their suitability for crop growth in the perspective of future space farming on Mars. The importance of simulants in validating scientific hypotheses is witnessed by the existence of a database which stores and regularly updates the available information on planetary simulants (The CSM Planetary Simulant Database; https://simulantdb.com/).

To evaluate the feasibility of using Lunar or Martian regolith simulants for crop growth, a thorough understanding of the physico-chemical properties of the substrates is needed, such as composition, water-holding capacity, porosity (Duri et al., 2022).

A very recent paper reported the major transcriptional changes of thale cress grown on different Lunar regolith samples from Apollo 11, 12 and 17, as well as the simulant JSC-1A (Paul et al., 2022); the results showed that although germination occurred for all the seeds on the different substrates, stunted roots developed in plants grown on real Lunar regoliths as compared to the simulant, accompanied by a slower growth of the aerial parts beyond day 8. From the transcriptional point of view, genes involved in stress response (salt, metal and reactive oxygen species-ROS stresses) were upregulated in the plants grown on the Apollo regolith samples, with the highest number of differentially expressed genes in the aerial tissues of plants grown on Apollo 11 regoliths and the lowest on Apollo 17 (Paul et al., 2022).

Although previous studies reported that plants can grow on Martian regolith simulants because of the presence of some essential nutrients (Wamelink et al., 2014), the lack of reactive N and the presence of perchlorate in native Martian regoliths are major limitations for plant growth (Oze et al., 2021).

Studies have demonstrated that reactive N can be provided by mixing regolith simulants with organic matter: the growth of different plant species, such as tomato, rye, quinoa, pea, radish was investigated on Martian regolith simulants mixed with mown shoot tissues of *Lolium perenne* L. as source of organic matter (Wamelink et al., 2019). The authors reported that the organic matter helped the germination and growth of all the plants studied and, for several of them, it was possible to collect fruits and seeds. Another very recent study has shown the feasibility of using alfalfa biomass to amend basaltic regolith simulants reproducing the real Martian surface (Kasiviswanathan et al., 2022): alfalfa grew on the nutrient-poor substrate when watered with *Synechococcus*-desalted briny water simulant and its biomass could be successfully used as biofertilizer to support the production of turnip, radish and lettuce on the basaltic regolith simulant.

In order to advance in space farming, it will be necessary to carry out investigations on substrates mimicking as closely as possible the real Martian (for example, the presence of perchlorate will have to be taken into account) or Lunar regoliths in conjunction with partial gravity. A recent study investigated the different molecular responses of thale cress seedlings exposed to Mars partial gravity and microgravity during spaceflight and revealed that red photostimulation helped overcome the stress effects of the spaceflight environment (Villacampa et al., 2021). Red light exposure impacted root nucleolar activity as evidenced by the increased size compared to non-exposed samples; Mars gravity triggered the overexpression of WRKY transcription factors known to be involved in (a)biotic stress response (Villacampa et al., 2021).

Although these results have demonstrated that it is possible to cultivate plants on Martian regolith simulants, molecular data obtained via proteomics and transcriptomics are missing. Obtaining such data provides useful information about the major gene ontologies/biochemical pathways intervening during the growth of plants on an alkaline substrate with low nutrient availability such as Martian regoliths. Such molecular data can also help devise plant biotechnology approaches to improve growth (Llorente et al., 2018).

To study the impact of Martian regolith simulants on the development of vegetative organs, as well as the expression of genes and the abundance of proteins, *L. multiflorum* Lam. (a.k.a. Italian ryegrass) was chosen as plant model. It is a representative of the economically relevant family Poaceae and a good example of fast-growing herbaceous species.

The plants were grown on potting soil and MMS-1 regolith simulant (Mojave Mars Simulant, coarse-grade) for a total of 14 days: leaves were sampled from plants grown for 7 and 14 days and for 7 days after performing a cut. The cut was carried out to understand how the plants would react and to have an estimation of the growth in a hypothetical scenario where ryegrass is mown to obtain organic matter for regolith amendment.

Gene expression analysis together with shotgun proteomics were performed on leaves and roots. Additionally, light microscopy observations were carried out on roots and leaves after 14 days of growth. Some physico-chemical analyses were also performed on the substrates and leachates: pH determination and elemental composition.

The analyses here provided will be useful for future studies on other species and will inspire biotechnological strategies aimed at improving plant growth performance on MMS-1.

2. Materials and methods

2.1. Plant growth and sampling

Seeds of *L. multiflorum* were germinated for one week on four layers of cotton tissue imbibed with distilled water and placed in a Petri plate (100 × 15 mm) in the dark at 25 °C. Eighteen conical 50 ml-tubes with skirt containing a layer of folded Miracloth at the bottom were placed in

Petri plates (60 × 15 mm) after having cut a hole in the lid with an electric welder, following the set-up described by Pétriacq and colleagues (Pétriacq et al., 2017). The tubes were pierced at the bottom, so that deionized water could be taken up from the Petri plates through the small holes and were wrapped in aluminium foil. Two sets of nine tubes were filled to the top with potting soil and MMS-1 (coarse-grade, purchased at The Martian Garden, https://www.themartiangarden.com/mms1/mms1) (Supplementary Fig. 1). The potting soil was prepared by mixing 1/3 sand (Agricon, Wirges, Germany) and 2/3 peat moss tourbe (Compo Deinze, Belgium) supplemented with perlite, fertilizer (1.1 kg/m^3 NPK with magnesium 14–16-18 + (2MgO), urea formaldehyde 0.2 kg/m^3) and oligoelements (0.1 kg/m^3 B, Cu, Fe, Mn, Mo, Zn). After 1 week, two plantlets were transferred to each tube and grown in a climatic chamber (Fitotron, Weiss Technik, Reiskirchen, Germany) under controlled conditions (photoperiod 16 h 25 °C/8 h 20 °C, 60 % relative humidity-RH) for a total of 14 days.

The plants were watered from the bottom of the tubes every three days with 25 ml deionized water. Watering was performed with deionized water to avoid providing nutrients eventually present in tap water (Wamelink et al., 2014). The leaves were sampled 7 days after cutting one plant per tube; the cut plants were then let regrow the leaves for 7 days (Supplementary Fig. 1). Leaves were finally sampled from 14-week-old plants, as well as from the cut plants. At the end of the experiment a total of three leaf sample types was thus collected, i.e., 7, 14 days old and 7 days after the cut. Roots were quickly separated using a razor blade after having carefully removed any soil/simulant particles and then immediately frozen in liquid nitrogen. The samples consisted of three biological replicates composed of 3 plants each. The leaf and root tissues were ground to a fine powder using liquid nitrogen and stored at −80 °C until RNA/protein extraction.

2.2. Sample preparation for light microscopy

Sections of leaves (about 2 × 2 mm) and roots (ca. 5 mm in length) were carefully excised from 14-day-old plants and directly observed with a light microscope (Olympus BX51, Tokyo, Japan) or dipped for 24 h at 4 °C in fixative solution (200 mM phosphate buffer pH 7.2, paraformaldehyde 2 % w/v, glutaraldehyde 1 % v/v, caffeine 1 % w/v). The samples were then cut to 10 μm-sections using a microtome (Leica Biosystems, Nussloch, Germany) and stained using FASGA, following the method described by Tolivia (Tolivia and Tolivia, 1987).

Root and leaf semithin sections were prepared by embedding the tissues in 5 % (*w/v*) agarose and by cutting them with a vibratome (Leica Biosystems, Nussloch, Germany). Iron deposits were detected using the Perls staining on freshly sliced unfixed root samples, as decribed previously (Green and Rogers, 2004) and then observed with the light microscope.

2.3. Substrate pH measurements

Three samples of growth substrate from each replicate were collected and dried at 50 °C for 72 h. Then 5 g from each sample were mixed with 30 ml of Milli-Q water (Merck, Kenilworth, NJ, USA). The samples were agitated for 1 h at room temperature. The pH was measured using an inoLab Multi 9430 IDS (WTW, Weilheim, Germany), as previously described (Guerriero et al., 2017).

2.4. Leachate collection and elemental analyses

Leachates were collected from potting soil and MMS-1 simulant without and with plants grown for 7 and 14 days by adding 5 ml of 50 % (v/v) methanol with 0.05 % (v/v) of formic acid from the top of the tube and collecting the flow-through in a tube at the bottom. This method was previously developed for the extraction of metabolites from non-sterile rhizosphere soil (Pétriacq et al., 2017). Four ml and a half were collected and centrifuged 5 min at 12000 rpm at room temperature. Then 4 ml were collected taking care to avoid withdrawing the pelleted particulate and 100 μl of HCl 1 M were then added (to avoid microorganisms' growth). Samples were frozen in liquid nitrogen and stored at −80 °C until analysis. Total elemental concentrations in potting soil and MMS-1 were determined on 0.5 g of sample after calcination at 450 °C for 24 h, followed by a $LiBO_2/Li_2B_4O_7$ fusion at 1000 °C for 5 min in a graphite crucible. After dissolution of the fusion residue in 100 ml of 10 % HNO_3, elemental concentrations (Al, Ca, Fe, K, Mg, Mn, Na, P, Si, Zn) were measured by ICP-AES (Agilent 5100/5110 VDV ICP-OES).

2.5. Gene expression analysis

RNA extraction from leaves was carried out with the RNeasy Mini Kit (Qiagen, Leusden, The Netherlands) following the manufacturer's instructions. RNA purity/integrity measurements, cDNA synthesis and qPCR were performed as previously described (Berni et al., 2021). A melt curve analysis was performed at the end of the PCR cycles to check the specificity of the primers. The primer efficiencies were determined using a calibration curve consisting of a serial dilution of 6 points (10, 2, 0.4, 0.08, 0.016, 0.0032 ng/μl). The normalized relative quantities (NRQs) were determined with qBase^{PLUS} (version 3.2, Biogazelle, Ghent, Belgium) by using *LmIF4A* and *LmTBP1* as reference genes for the leaves sampled at 7 days, *LmIF4A* and *LmE2* for the leaves at 14 days, *LmE2* and *LmGAPDH* for the leaves regrown after the cut. The reference genes were selected according to geNORM (Vandesompele et al., 2002). The target genes were selected starting from a *de novo* assembly generated by using raw data present in the Sequence Read Archive-SRA repository (SRR3100237, SRR10984852, SRR3194161) (Hu et al., 2020; Pan et al., 2016). Sequences were uploaded in CLC Genomics Workbench v. 11.0.1 (QIAGEN Aarhus A/S, Denmark) and filtered as follows: sequences >35 bps, the sequence quality score was left as default value (0.05), the maximum number of ambiguities was set to 0. The sequences were trimmed of 15 bps at the 5′ end and 3 bps at the 3′ end. The parameters used for the *de novo* transcriptome assembly were as follows: wording size was set to 20, the bubble size to 50 and minimum contig length to 300. The reads were mapped back to the assembly with a mismatch, insertion and deletion cost of 3 (stringent criteria) and a length and similarity fraction of 0.95. The assembly was then annotated using FunctionAnnotator (Chen et al., 2017) (http://fa.cgu.edu.tw/) against the *Viridiplantae* non-redundant database. For each of the 12 libraries, the mapping was performed with a maximum hit per read of 3, a similarity and length fraction of 0.95, a mismatch, insertion and deletion cost of 3. The annotation and FASTA sequences are available as supplementary files (Supplementary File 1 and 2).

Genes of interest were obtained by blasting the annotated sequences against thale cress, *Oryza sativa*, *Hordeum vulgare* and *L. perenne* sequences by querying different databases, namely NCBI and Phytozome. To get an estimation of the gene expression in the vegetative tissues of other plants (either dicots and monocots), the eFP browser was queried for thale cress, *Brachypodium distachyon*, *Triticum aestivum* and *Oryza sativa*, available at http://bar.utoronto.ca/.

The specificity of the primers on redundant families of genes was evaluated by performing multiple alignments through CLUSTAL-Ω (http://www.ebi.ac.uk/Tools/msa/clustalo/).

The primers were designed using Primer3Plus (http://www.bioinformatics.nl/cgi-bin/primer3plus/primer3plus.cgi) and verified with the OligoAnalyzer 3.1 tool from Integrated DNA Technologies (http://eu.idtdna.com/calc/analyzer). All the primers and their relative features (sequences, Tm, amplicons' size, amplification efficiency and R^2) are reported in Supplementary Table 1.

Principal Component Analysis (PCA) was performed with ClustVis (https://biit.cs.ut.ee/clustvis/) (Metsalu and Vilo, 2015).

The hierarchical clustering of the qPCR data (presented as heatmaps) was carried out with Cluster 3.0 (Eisen et al., 1998) and visualized with Java Treeview (Saldanha, 2004) (available at http://jtreeview.sourceforge.net/).

2.6. Shotgun proteomics

Approximately 50 mg of ground leaf and root tissues were taken for each sample and dissolved in 100 μl of Lyse buffer provided in the PreOmics iST Kit (PreOmics GmbH; Martinsried, Germany). The samples were

incubated at 70 °C for 10 min and continuously shaken at 1000 rpm. Then the samples were transferred into a BeatBox tissue homogenizer (PreOmics GmbH; Martinsried, Germany) to favor the complete lysis of the material. The roots and leaves were homogenized for 10 min using 2 different intensities, i.e., high for the roots and standard for the leaves because these parameters gave the best results in terms of number of proteins identified in the two tissues, according to initial analyses. The extracted proteins were quantified using the Bradford method (Bradford, 1976), with BSA for the standard curve. Fifty μg of total proteins of each sample were digested and processed following the manufacturer's protocol (BeatBox and iST Tissue Kit 96x, PreOmics GmbH; Martinsried, Germany).

LC-MS analysis was performed on a NanoLC-425 Eksigent system coupled to TripleTOF® 6600 + mass spectrometer and carried out as previously reported (Guerriero et al., 2021; Xu et al., 2021). The acquired MS and MS/MS data were imported in Progenesis QI for Proteomics software (version 4, Nonlinear Dynamics, Waters, Newcastle upon Tyne, UK). The protein and peptide identifications were done by searching the Pooideae database on UniprotKB (downloaded on 28-06-2022) via Mascot Daemon (version 2.6.0. Matrix Science, London, UK) and matched to the peptide spectra. The Mascot research parameters were: peptide tolerance of 20 ppm, fragment mass tolerance of 0.3 Da, max two missed cleavages, carbamido-methylation of cysteine as fixed modification and oxidation of methionine, N-terminal protein acetylation and tryptophan to kynurenine as variable modifications. The three biological replicates were merged. Only the proteins identified with a significance Mascot-calculated confidence of 95 %, minimum of two peptides, at least one unique per proteins and an ANOVA p-value < 0.05 were retained. The proteomics data were deposited in the ProteomeXchange Consortium via the PRIDE partner (Vizcaíno et al., 2016) repository with the dataset identifier PXD035041 and https://doi.org/10.6019/PXD035041.

PCA and hierarchical clustering of the protein abundances (presented as heatmaps) were obtained as described in Section 2.5 for the qPCR data.

2.7. Statistical analyses

Data were log2-transformed and analyzed with IBM SPSS Statistics v20 (IBM SPSS, Chicago, IL, USA). Normal distribution of the data was checked with the Shapiro-Wilk test and graphically with a Q-Q plot. Homogeneity of the data was checked with the Levene's test. For data following normal distribution and homogeneous, a one-way ANOVA with Tukey's post-hoc test was performed. For data not following normal distribution and/or not homogeneous, a Kruskal-Wallis test was performed with Dunn's post-hoc test.

3. Results

3.1. Observations of phenotypes at the light microscope

The plants grown on potting soil and MMS-1 will be hereafter indicated with the abbreviations PGS and PGM, respectively. Compared to PGS (Fig. 1A), the leaves of PGM showed extensive yellowing of the tissues starting from the external margins of the lamina towards the central vein (Fig. 1C). In cross section, the xylem in the central vein of PGM leaves was less developed (Fig. 1D) with a narrower lumen of the vessels compared to PGS (Fig. 1B) and thicker cuticle of the epidermal cells (insets in Fig. 1B and D). The leaves in PGM were also bent downwards (Fig. 1D).

Roots of PGM showed brownish deposits reminiscent of ferritin accumulation (Fig. 2D) that were not observed in PGS (Fig. 2A). To verify whether they corresponded to Fe deposits, PGM roots were incubated with the Perls reagent which stains Fe deposits blue: blue spots were observed in proximity of the brownish aggregates (inset in Fig. 2D).

The apex of PGM roots showed fewer border cells (Fig. 2E) compared to PGS (Fig. 2B). Microtome sections of roots sampled from PGM allowed the identification of a clear phenotype, i.e., the presence of lacunae (Fig. 2F, asterisks). Lacunae are not present in roots from PGS (Fig. 2C) where the cortex is continuous. While the central vascular tissue of PGM is much smaller

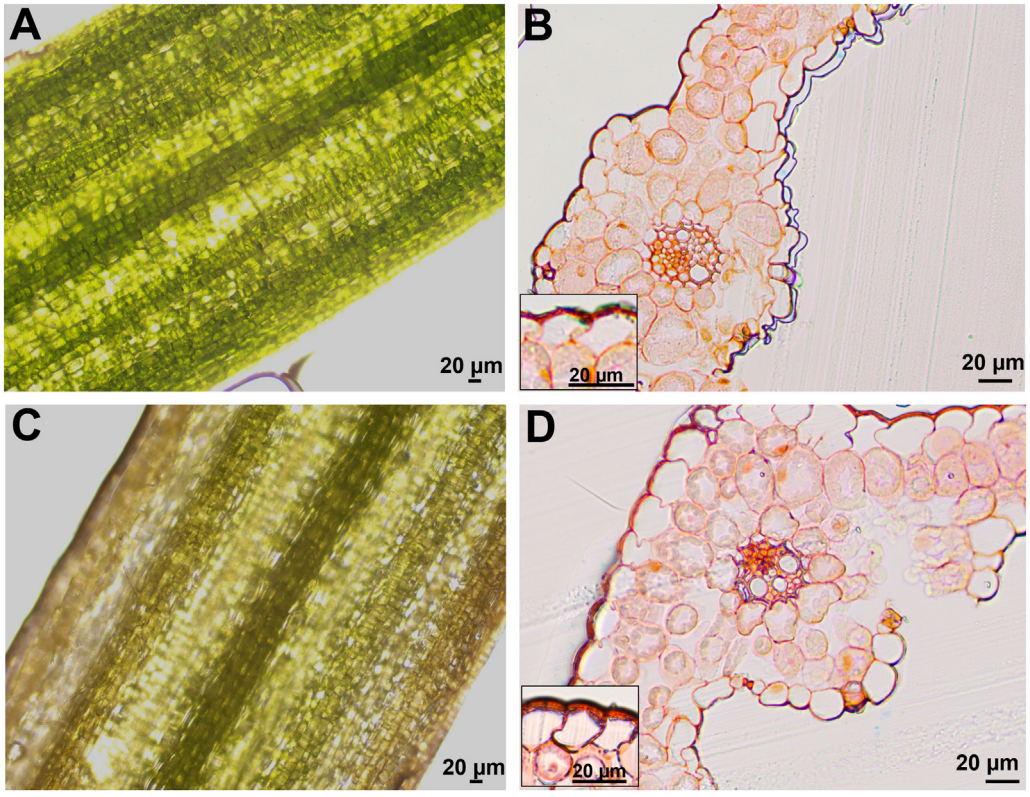

Fig. 1. Light microscope pictures of PGS and PGM leaves. A: Dorsal view of a PGS leaf; B: Thin slice of a PGS leaf stained with FASGA; C: Dorsal view of a PGM leaf with pronounced discoloration; D: Thin slice of a PGM leaf stained with FASGA (note downward bending of the lamina). Insets in B and D: Details of the cuticle stained with FASGA.

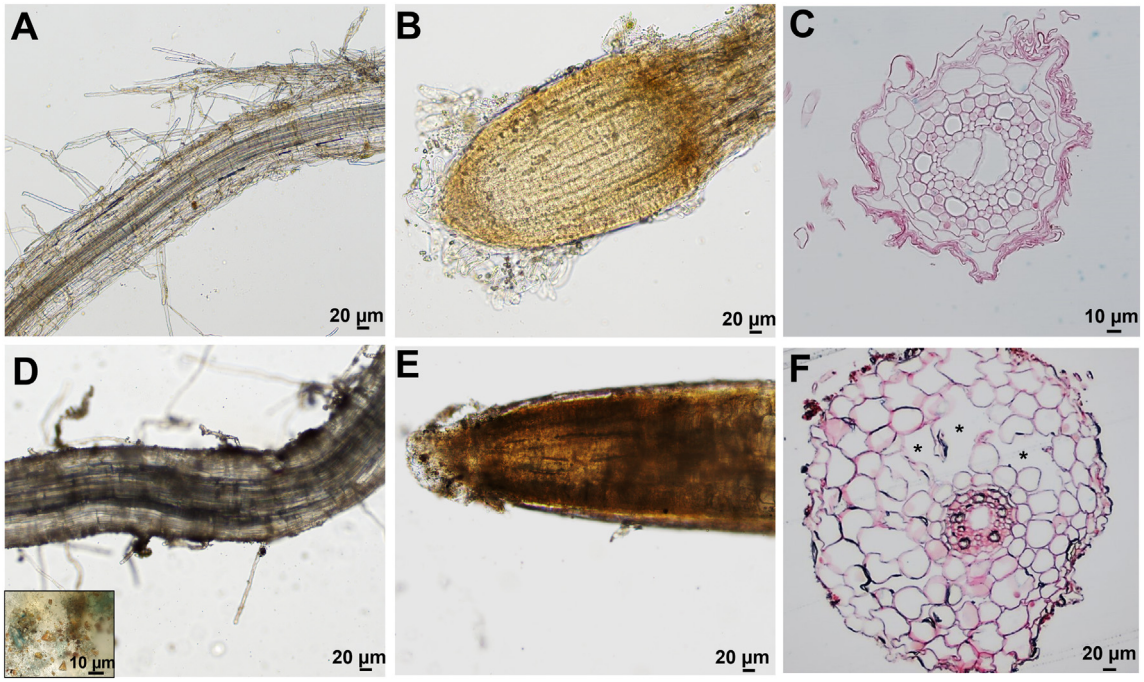

Fig. 2. Light microscope pictures of PGS and PGM roots. A: View of a PGS root; B: Apex of a PGS root with border cells; C: Thin slice of a PGS root; D: View of PGM root; E: B: Apex of a PGM root; F: Thin slice of a PGM root (note the lacunae indicated by the asterisks). Inset in D: Details of the ferritin-like deposits stained blue by the Perls reagent.

than PGS roots, the root parenchyma of plants grown on MMS-1 is more developed (Fig. 2C and F).

3.2. Physico-chemical analyses of potting soil and MMS-1

An elemental analysis of the 2 substrates used for plant growth was performed: (Table 1). The overall elemental composition of MMS-1 was higher than that of potting soil. More specifically, MMS-1 coarse-grade consists in majority of Si, Al and Fe (in g/kg), but also contains other elements which are important for the growth of plants, namely Ca, K, Mg, Na and P.

In order to understand whether the growth of plants on MMS-1 triggered any root-associated processes, the elemental composition of the potting soil/MMS-1 leachates was investigated. The leachates were collected from tubes containing *Lolium* grown for 7 and 14 days (7d and 14d), as well as from control tubes without any plants. The concentration of P, Mn, K, was significantly higher in leachates obtained from potting soil (Fig. 3). Higher concentrations were also measured in leachates obtained from potting soil for Ca, Mg, Zn, although the differences compared to MMS-1 were not significant. The abundance of the elements (except for K) did not show significant differences in the leachates from potting soil/MMS-1 at the two sampling points of 7d and 14d compared to the respective controls without plants. Fe could only be detected in leachates from regolith simulants without plants (Fig. 3B).

MMS-1 showed a pH value of 9.25 ± 0.17 (n = 3), while the potting soil had pH 4.87 ± 0.16 (n = 3). After 14 days of plant growth, the pH of MMS-1 decreased to 8.55 ± 0.21 (n = 3), while the pH of the potting soil increased to 5.29 ± 0.11 (n = 3) (statistical parameters: pH $X^2(3) = 10.385$, $p = 0.016$).

3.3. Gene expression analysis

Since the molecular processes involved in plant growth on MMS-1 are still unknown, genes partaking in primary metabolism/nutrition (sucrose synthases-*SuSy*, Fd-dependent glutamate synthase-*Fd-GOGAT*, asparagine synthetase-*ASNS*, phosphate starvation response-*PHR*, Fe transport-*YSL*, chlorophyll biosynthesis-*MgCHLI1*), stress response (Fe-superoxide dismutase-*FeSOD*, ascorbate peroxidase-*APX*, catalase-*CAT*) and phenylpropanoid pathway (phenylalanine ammonia lyase-*PAL*, cinnamyl alcohol dehydrogenase-*CAD*, hydroxycinnamoyl-CoA: shikimate hydroxycinnamoyl transferase-*HCT*) were targeted.

The PCA of the gene expression data in the leaf samples was performed to check if the two groups, PGM and PGS, were well separated (Supplementary Fig. 2). The first two components of the PCA, PC1 and PC2, explain 62.4 % of the total variance, with PC1 and PC2 explaining 40.8 % and 21.6 %, respectively. Two well-separated groups can be distinguished, one for PGM and one for PGS leaves; a less clear grouping of the time-points is present within each group, although an overall better separation into three sub-groups is present for PGM samples.

Fig. 4 shows the presence of three main gene expression clusters, hereafter referred to as C1-C3. Genes belonging to C1 show the highest expression in PGM at 14 days of growth and after 7 days of regrowth after the cut. C1 includes *SuSy6*, *ASNS1*, *SuSy1*, *PAL1-5*, *YSL13*, *CAD1*, *APX2* and *CAT2-2*. C2 includes *SuSy4*, *YSL14*, *PHR1*, *APX1*, *PAL1-4*, *Fd-GOGAT*, *APX4* and *HCT1-3* and the genes in this cluster show the lowest expression in PGM. The last cluster, C3, comprises *MgCHLI1*, *FeSOD1* and *FeSOD2*. C3 displays no differences at 7 days of growth in PGM and PGS, while opposite trends are observed at 14 days and 7 days after the cut.

Table 1
Elemental composition of potting soil and MMS-1 (n = 3). The values are given in g/kg (± SD).

	Al	Ca	Fe	K	Mg	Mn	Na	P	Si
					(g/kg)				
MMS-1	76.72 ± 5.07	40.46 ± 2.49	51.30 ± 2.32	19.13 ± 0.48	17.06 ± 0.62	0.9 ± 0.05	2.14 ± 0.06	1.39 ± 0.09	259.68 ± 11.32
Soil	3.76 ± 0.14	7.22 ± 0.53	1.24 ± 0.07	2.68 ± 0.17	0.55 ± 0.03	0.02 ± 0.00	0.11 ± 0.01	0.31 ± 0.03	112.25 ± 29.97

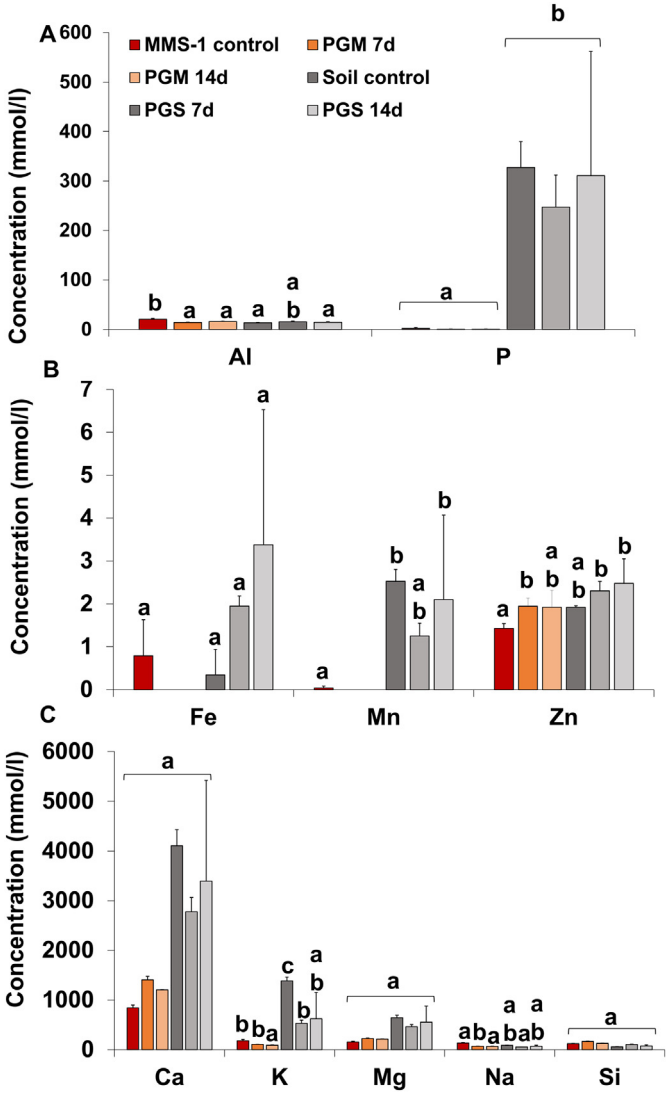

Fig. 3. Elemental concentrations of potting soil/MMS-1 leachates without (MMS-1 Control and Soil Control) and with plants grown for 7 and 14 days (PGM/PGS 7d and 14d). The different letters on the vertical bars indicate statistically significant differences among groups ($p < 0.05$). Statistical parameters: A) Al $X^2(5) = 15.302$, $p = 0.009$, P $X^2(5) = 15.423$, $p = 0.009$, Fe $X^2(5) = 1.800$, $p = 0.867$, Mn $X^2(5) = 15.300$, $p = 0.009$, Zn $X^2(5) = 12.000$, $p = 0.035$, Ca $X^2(5) = 9.536$, $p = 0.089$, K $X^2(5) = 11.522$, $p = 0.042$, Mg $X^2(5) = 7.161$, $p = 0.209$, Na $X^2(5) = 13.789$, $p = 0.017$, Si $X^2(5) = 9.067$, $p = 0.106$.

Indeed, while in PGM the expression values are the highest at 14 days, in PGS the 3 genes are down-regulated; at 7 days after the cut, the genes are down-regulated in PGM and induced in PGS. The bar charts of the normalized gene expression data with statistical significance are available in Supplementary Fig. 3.

3.4. Protein profiles in leaves and roots of plants grown on potting soil and MMS-1

A proteomic approach was here adopted to complement the qPCR analyses and to understand the major biochemical pathways occurring in the leaves and roots during growth on MMS-1. The PCA of the most abundant significant proteins (Supplementary File 3) revealed a good separation between PGM and PGS (Supplementary Fig. 4). The first two components of the PCA obtained with the root samples explains 91.3 % of the total variance, with PC1 and PC2 explaining 82.2 % and 9.1 %, respectively (Supplementary Fig. 4A). In the leaves, the PCA explains 87.9 % of the total variance, with PC1 and PC2 explaining 78.3 % and 9.6 %, respectively (Supplementary Fig. 4B). In both PCAs, the PGM replicates cluster tightly together, while a higher scattering is present for PGS.

In the roots, a total of 73 differentially abundant proteins was detected, while in the leaves 37 were obtained using the above-mentioned selection criteria (Supplementary File 3). A hierarchical clustering of the heatmaps was drawn to detect the clusters of proteins showing a similar expression profile. In the roots, 5 clusters were obtained by choosing a Pearson's correlation coefficient > 0.5 (Fig. 5). The first 4 clusters share a pattern characterized by a higher abundance in PGS: cluster 1 with 4 proteins, cluster 2 with 35, cluster 3 with 8 and cluster 4 with 21. The last cluster comprises 5 proteins with higher abundance in PGM (Supplementary File 3).

In the leaves, the hierarchical clustering revealed the presence of 4 clusters with a Pearson's coefficient > 0.7 (Fig. 6): clusters 1 and 2 group proteins found at higher levels in PGM (10 and 8, respectively), while clusters 3 and 4 (11 and 8 proteins, respectively) are characterized by a higher abundance in PGS leaves.

Among the proteins showing the highest abundance in PGS roots (fold change-FC ≥ 30 with respect to PGM roots) there are proteins involved in primary metabolism (C1 metabolism, energy production, TCA cycle), translation, cytoskeletal organization, as well as the ABA-responsive Late Embryogenesis Abundant (LEA) protein WRAB1 (Table 2). These proteins are found among clusters 1–4 (Supplementary File 3). In PGM roots, 4 proteins with FC ≥ 2 belonging to cluster 5 and involved in C1 metabolism (methylation), DNA binding and histone methylation are found (Table 2).

In PGS leaves the most abundant proteins are related to stress response, primary metabolism (photosynthesis, glycolysis), translation, ATP synthesis and they are distributed among clusters 3 and 4 (Table 3). In PGM leaves the most abundant proteins are in clusters 1–2 and are involved in stress response, cysteine biosynthetic process, photosynthesis, transcription regulation, protein degradation, vesicle transport, cytoskeleton organization and C1 metabolism (methylation) (Table 3).

4. Discussion

Roots and leaves of *L. multiflorum* showed alterations of their normal phenotype when grown on MMS-1 coarse-grade: chlorotic, bent leaves with a thicker cuticle were observed (Fig. 1), together with a lacunar aerenchyma in the roots (Fig. 2). MMS1-1 coarse-grade was characterized mainly by Si, Al, Fe, but also contained other elements important for the development of plants, namely Ca, K, Mg, N and P. These data are in agreement with what previously reported for MMS-1 fine-grade (Caporale et al., 2020).

Leaf rolling typically occurs under conditions of water deficit, as well as in the presence of abiotic (heavy metals, salinity, UV) and biotic stresses (Kadioglu et al., 2012). It is a mechanism of drought avoidance that aims at reducing the leaf area and transpiration. The occurrence of this phenotype in the aerial organs can be linked to the lacunar aerenchyma in PGM roots. Root cortical lacunae develop in response to waterlogging or flooding conditions and allow an adequate oxygen supply (Ni et al., 2019). Root aerenchyma also occurs in case of nutrient deficiencies (Hu et al., 2014; Postma and Lynch, 2011) and is an adaptive mechanism allowing plants to reduce the cost of root maintenance and favor soil exploration to enhance the acquisition of elements in deep soil strata (Saengwilai et al., 2014).

It was shown that cortical aerenchyma decreases radial water transfer via the symplastic and apoplastic pathways because of the reduced presence of living cells: the presence of lacunae favors gas diffusion at the expense of the vascular transport system (Ouyang et al., 2020). Macro- and micro-nutrients deriving from the degradation of organic matter are lacking in Martian regolith simulants (Duri et al., 2022) and this was confirmed by the elemental analysis (Fig. 3) where the concentration of the macronutrients P and K was significantly higher in leachates of potting soil. The scarcity of macronutrients is a possible a trigger for the development of the root aerenchyma observed in *L. multiflorum*. Root aerenchyma, in its turn, causes

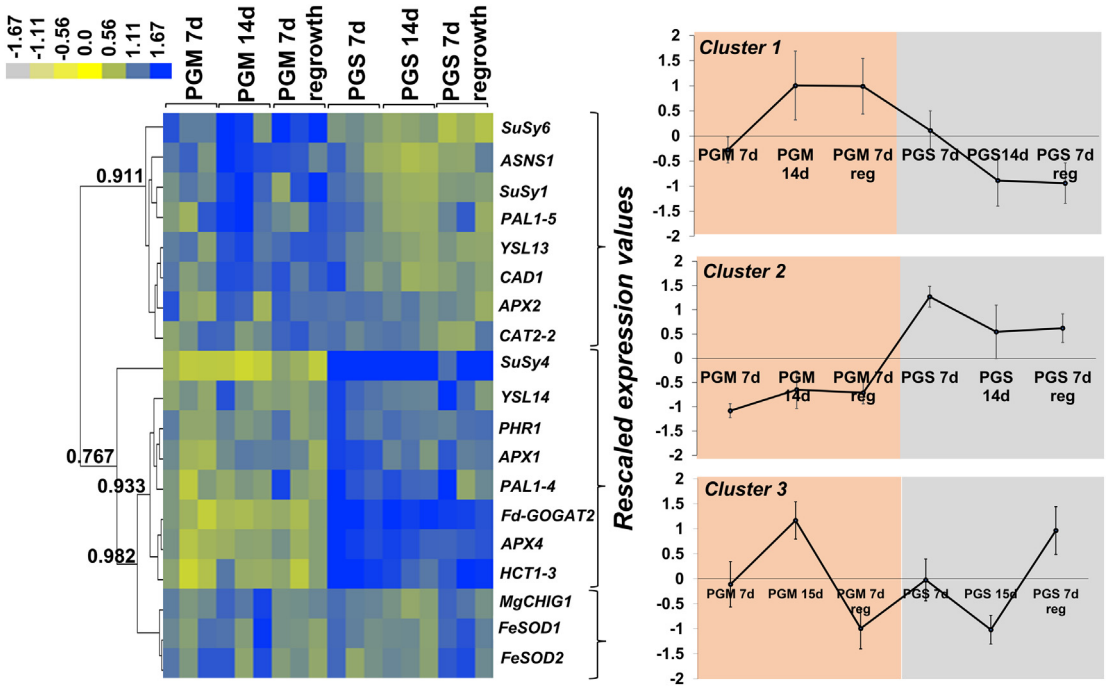

Fig. 4. Gene expression pattern in leaves of PGM and PGS. (a) Heat map hierarchical clustering of the qPCR data (the numbers on the branches indicate the Pearson's correlation coefficients). The scale bar indicates the pixel colour intensities which are directly proportional to the expression values. Clusters 1–3 show the rescaled expression values ± standard deviation (the rescaled values were obtained by subtracting from each expression value the average among the conditions and dividing by the standard deviation).

a reduced water transport to the aerial parts; consequently, the leaves bend downwards and thicken the cuticle to limit water loss.

The alkaline conditions imposed by MMS-1 can also explain the thickening of the cuticle: *Prunus triloba* under alkaline stress increased indeed the upper and lower epidermal cuticle (Liu et al., 2017).

The ferritin-like deposits detected in PGM roots stained blue with the Perls reagent, a result confirming the presence of Fe (Fig. 2D inset). The reagent stains mainly Fe(III)-ferric ion, e.g., ferritin and hemosiderin. At such an alkaline pH as the one measured in MMS-1 (pH 9.25), Fe is in the form of insoluble ferric oxide-Fe_2O_3 and poorly available for *L. multiflorum*. The analysis on MMS-1 leachates revealed the presence of Fe in the control samples (without plants), while in the leachates from PGM at 7d and 14d none was detected (Fig. 3B). This result shows that Fe was completely taken up by PGM roots and the presence of brownish Fe-containing deposits in PGM roots indicates that the uptaken Fe was subsequently stored. Since no organic matter was added to MMS-1, root processes can be the only means through which plants may have mobilised Fe. Grasses uptake Fe using strategy II which relies on the secretion of phytosiderophores-PS

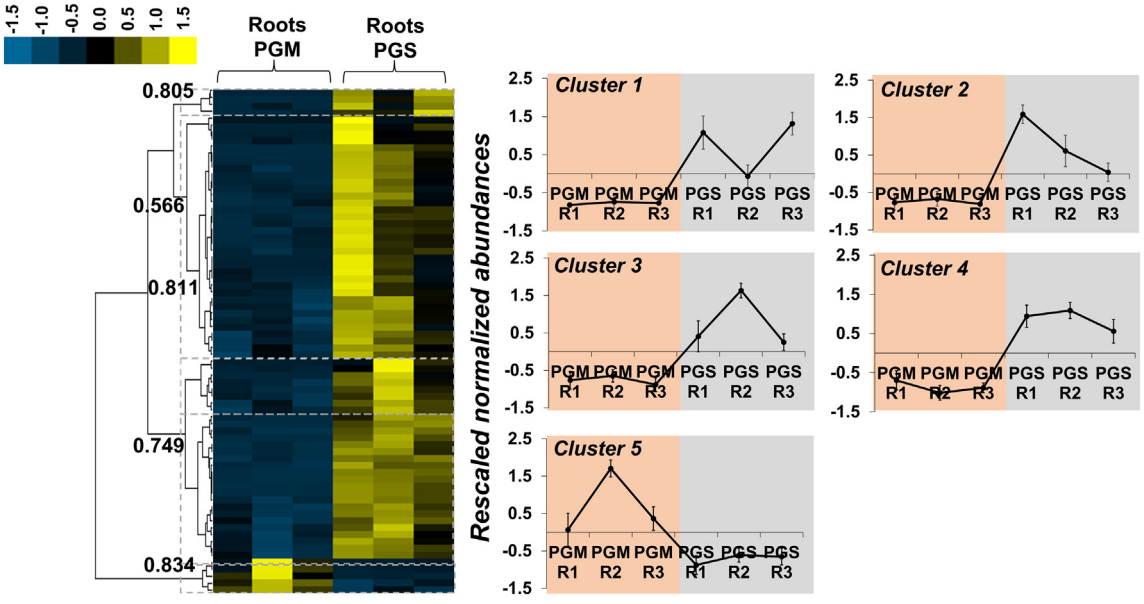

Fig. 5. Heat map hierarchical clustering of the protein abundances in PGM and PGS roots (the numbers on the branches indicate the Pearson's correlation coefficients). The scale bar indicates the pixel colour intensities which are directly proportional to the normalized abundances. The dotted boxes show the clusters with correlation coefficient > 0.5. Clusters 1–5 show the rescaled normalized abundance values ± standard deviation (the rescaled values were obtained by subtracting from each value the average among the conditions and dividing by the standard deviation).

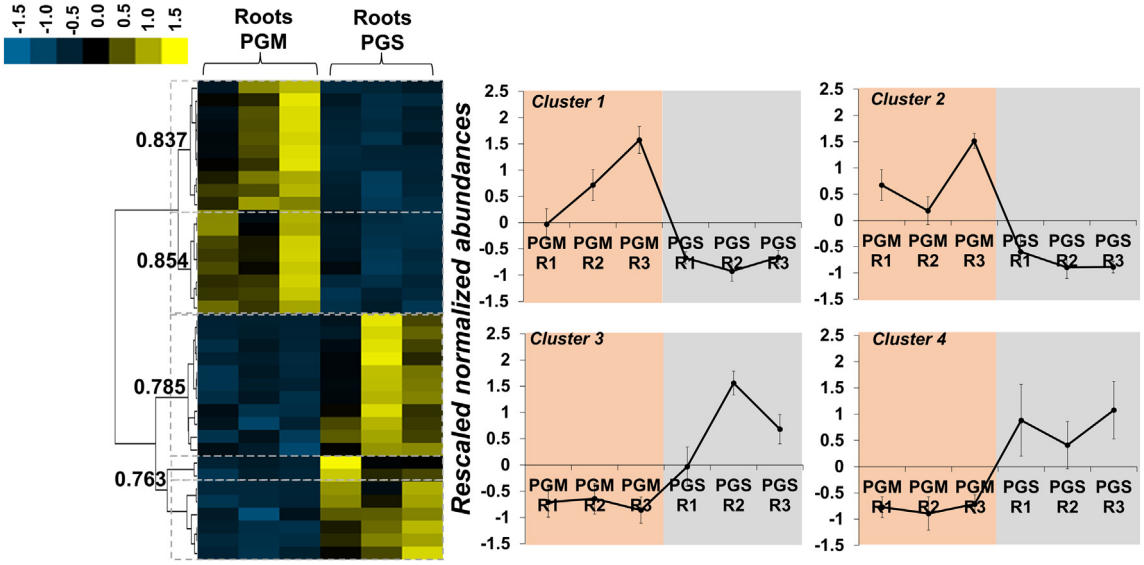

Fig. 6. Heat map hierarchical clustering of the protein abundances in PGM and PGS leaves (the numbers on the branches indicate the Pearson's correlation coefficients). The scale bar indicates the pixel colour intensities which are directly proportional to the normalized abundances. The dotted boxes show the clusters with correlation coefficient > 0.6. Clusters 1–4 show the rescaled normalized abundance values ± standard deviation (the rescaled values were obtained by subtracting from each value the average among the conditions and dividing by the standard deviation).

(e.g., mugineic acid). PS complex with Fe(III) and mediate its direct uptake through Yellow Stripe 1-YS1 transporters (Curie et al., 2001). PS are secreted in the rhizosphere under Fe deficiency (Römheld, 1991). The low availability of Fe due to the alkaline pH of MMS-1 may have caused Fe deficiency stress and induced PS production for the uptake and the sequestration of Fe(III) in the form of deposits in PGM roots. The qPCR data (Supplementary Fig. 3) support the existence of Fe deficiency stress in PGM. Genes involved in Fe uptake are usually up-regulated under Fe deficiency stress in monocot roots and shoots (Li et al., 2019; Zhang et al., 2018). *YSL* belong to the YS transporter family mediating the uptake of PS-Fe(III) complex (Curie et al., 2009, 2001) and phylogenetic analyses have revealed the existence of several members whose role is also in the transport of other metals, such as Cu (Dai et al., 2018; Zheng et al., 2012). In PGM leaves, *YSL13* increased in expression while *YSL14* did not show significant changes compared to PGS leaves, except for the time point at 7 days after the cut (Supplementary Fig. 3).

Table 2
Subset of proteins found in higher abundance in PGS (FC ≥ 20) and PGM roots (FC ≥ 2).

Accession	Description	Fold change norm. abundance PGS roots vs PGM roots	Function	Cluster
Higher abundance in PGS				
A0A452ZCB3_AEGTS	Aldo_ket_red domain-containing protein	∞	Secondary metabolites biosynthesis, transport and catabolism	1
A0A3B5ZQE8_WHEAT	Ribosomal_L18e/L15P domain-containing protein	∞	Translation	2
F2DAK3_HORVV	Ribosomal protein eL6 family	∞	Translation	2
A0A1D5UPW5_WHEAT	Serine hydroxymethyltransferase	∞	C1 metabolism	2
A0A446P284_TRITD	Cytochrome c domain-containing protein	∞	Electron transfer	2
A0A2K2D782_BRADI	Ribosomal protein uL5 family	∞	Translation	2
I1H4V9_BRADI	40S ribosomal protein S6	∞	Translation	2
Q9XFD0_WHEAT	ABA-inducible protein WRAB1	∞	Stress response	3
I1H5X4_BRADI	Uncharacterized protein (similar to Ricin B-like lectin EULS3-like)	∞	Lectin binding carbohydrates	3
A0A446QRW9_TRITD	UDP-glucuronate decarboxylase	224.3	Xylan biosynthesis	2
A0A446T628_TRITD	Heat shock protein 90 family	123.6	Protein folding	2
TBB2_WHEAT	Tubulin beta-2 chain	69.2	Cytoskeletal functions	2
A0A8F5V7F2_9POAL	ATP synthase protein MI25	65.1	ATP synthesis	1
A0A3B5XUT5_WHEAT	Dihydrolipoyl dehydrogenase	42.3	TCA cycle/photrespiration/ degradation of branched-chain α-ketoacids	2
A0A3B6QKK6_WHEAT	Aldedh domain-containing protein	38.5	Reactive aldehydes detoxification	1
A0A3B6ASV4_WHEAT	Ribosomal protein eL22 family	35.8	Translation	4
A0A8I6Y0I2_HORVV	3-ketoacyl-CoA synthase 4-like	31.4	Fatty acid biosynthetic process	3
A0A3B6HW60_WHEAT	Phosphoglucomutase	29.9	Carbohydrate metabolic process	2
A0A3B6NTT8_WHEAT	Annexin	28.5	Response to stress	4

Accession	Description	Fold change norm. abundance PGM roots vs PGS roots	Function	Cluster
Higher abundance in PGM				
A0A446R6W8_TRITD	Serine hydroxymethyltransferase	9.7	C1 metabolism	5
Q4LB20_HORVU	Adenosylhomocysteinase	7.7	C1 metabolism	5
A0A446UDK7_TRITD	Bromo domain-containing protein	2.6	DNA binding (epigenetic regulation)	5
A0A0Q3FDW2_BRADI	SET domain-containing protein	2.0	Histone methylation	5

Table 3
Subset of proteins found in higher abundance in PGS (FC ≥ 2) and PGM leaves (FC ≥ 2).

Accession	Description	Fold change norm. abundance PGS leaves vs PGM leaves	Function	Cluster
Higher abundance in PGS				
A0A0Q3K0U1_BRADI	Uncharacterized protein (similar to LEA type 4 family)	166.3	Stress response	3
A0A1D5ZGE0_WHEAT	Fructose-bisphosphate aldolase	61.1	Glycolysis	4
A0A3B6HVT4_WHEAT	Vicilin-like seed storage protein	35.9	Seed storage protein	3
A0A453MRM4_AEGTS	MADS-box domain-containing protein	11.9	DNA binding	4
I1IE72_BRADI	50S ribosomal protein L9, chloroplastic	4.6	Translation	3
A7KMF2_LOLPR	Eukaryotic initiation factor 4A	3.5	ATP binding	3
K4P9Z0_FESPR	Ribosomal protein L16	3.3	Translation	3
A0A446QVT1_TRITD	eIF2B_5 domain-containing protein	3.1	Translation initiation factor	4
A0A3B6FIG 0_WHEAT	Glutamate decarboxylase	2.7	Glutamate catabolic process	3
A0A3B6LP05_WHEAT	Peptidylprolyl isomerase	2.5	Peptidyl-prolyl *cis-trans* isomerase activity	4
A0A3B6HQW7_WHEAT	30S ribosomal protein S1, chloroplastic-like	2.4	*S*-adenosylmethionine-dependent methyltransferase activity	3
A0A3B6SNT5_WHEAT	F-box domain-containing protein	2.2	Protein-protein interaction	3
A0A3B6HZS2_WHEAT	1-phosphatidylinositol 4-kinase	2.0	Phosphatidylinositol phosphate biosynthetic process	3

Accession	Description	Fold change norm. abundance PGM leaves vs PGS leaves	Function	Cluster
Higher abundance in PGM				
A0A3B6HPZ5_WHEAT	Heat shock cognate 70 kDa protein-like	8.3	Stress response	1
M8BF24_AEGTA	Histone acetyltransferase HAC12	4.9	Histone acetylation	2
A0A3B6AV65_WHEAT	Plastoquinol-plastocyanin reductase	4.1	Photosynthesis	2
A0A8I6YKZ4_HORVV	REVEILLE 1-like	4.0	Transcription regulation	2
A0A0Q3E443_BRADI	Cysteine synthase	4.0	Cysteine biosynthetic process from serine	1
C9WWM9_DACGL	Cytosolic heat shock protein 90.2	3.8	Stress response	1
A0A3B6TKH9_WHEAT	Uncharacterized protein (similar to class I-like SAM-binding methyltransferase superfamily)	3.6	Methylation	1
A0A446WR03_TRITD	AP-1 complex subunit gamma	3.4	Vesicle-mediated transport	1
A0A8I7BBA7_HORVV	Villin-1	3.4	Cytoskeleton organization	2
A0A446R6W8_TRITD	Serine hydroxymethyltransferase	3.3	C1 metabolism	1
T1M863_TRIUA	Non-specific serine/threonine protein kinase	3.2	ATP and polysaccharide binding	2
Q4LB20_HORVU	Adenosylhomocysteinase	2.9	C1 metabolism	1
I1J0U4_BRADI	Ubiquitin fusion degradation protein 1 homolog isoform X1	2.6	ER-associated ubiquitin-dependent protein degradation	2
A0A1X9ZPN2_BROTE	Ribulose bisphosphate carboxylase large chain	2.1	Photosynthesis	1
R7WFC7_AEGTA	Uncharacterized protein (similar to pentatricopeptide repeat-containing protein)	2.0	Plant growth and development	1

The increased expression of *YSL13* indicates a response at the leaf-level to Fe deficiency stress.

Aspects warranting future investigations are the lowering of the pH and the trend towards an increase of some element concentrations (Ca, Mg, Si; Fig. 3) in MMS-1 leachates in the presence of plants. It is known that plant roots secrete protons and exude organic acids and this process impacts soil pH thereby affecting the mobilization of elements (Nardi et al., 2000). The results here obtained, despite the short timeframe of the experiment, show that growing *Lolium* on MMS-1 affects the pH of regolith simulants.

The leaf chlorosis observed in PGM due to the scarcity of macronutrients can be aggravated by the low availability of Fe at alkaline pH and the reduced vascular transport of water and nutrients caused by the root aerenchyma. In the leaves, Fe is associated with the chloroplasts and is important for the photosynthetic activity (Rodriguez-Celma et al., 2013), as it is a cofactor for the photosynthetic electron transfer reactions.

Fe is also involved in ROS defense mechanisms as an important constituent of heme group and cofactor for the proper functioning of ROS scavenging enzymes, such as APX, SOD and CAT (Santos et al., 2019). With the exception of *APX2* in plant leaves from PGM 7 days, the other transcripts encoding antioxidant enzymes either did not show statistically significant changes or were more expressed in PGS leaves (Supplementary Fig. 3). It should be noted that in thale cress, under Fe deficiency, *FeSOD*s were down-regulated and replaced by *CuSOD*s (Waters et al., 2012): a mechanism may thus be present in PGM which regulates the expression of genes coding for enzymes relying on Fe as cofactor.

Plants assimilate N through the enzyme-based system glutamine synthetase-glutamate synthase (GS-GOGAT). The lower expression of *Fd-GOGAT* in PGM leaves compared to PGS at 7, 14 days and 7 days after the cut is in line with the lack of reactive N in MMS-1. Among the N metabolism-related genes, asparagine synthetase (*ASNS*) showed significantly higher expression in PGM leaves after 14 days of growth (Fig. 4 and Supplementary Fig. 3). Asparagine acts as N storage and transport molecule (Lea et al., 2007) and its accumulation was shown to increase under conditions of S deficiency in wheat (Gao et al., 2016). MMS-1 lacks S (Caporale et al., 2020) and this deficiency can account for the increased expression of *ASNS1* in PGM leaves. Another aspect to consider is that, under N scarcity, leaf premature senescence may be triggered as reported in rice (Zakari et al., 2020) and the ammonia liberated by proteolysis detoxified via the enzymatic action of ASNS (Oddy et al., 2020).

P deficiency causes a molecular signaling orchestrated by the phosphate starvation response gene (*PHR1*), described as the central regulator of plant transcriptional responses (Rubio et al., 2001; Sega and Pacak, 2019). Despite the lower P concentration in MMS-1 leachates compared to potting soil, PGM and PGS leaves showed a similar expression of *PHR1*, except at 14 days, where the expression was significantly lower in PGM (Supplementary Fig. 3). The absence of major transcriptional changes in *PHR1* under varying phosphate regimes was observed in other plants, both monocots (barley) and dicots (thale cress) (reviewed by Sega and Pacak, 2019).

With respect to chlorophyll biosynthesis, the enzyme Mg-chelatase plays a crucial role, by inserting Mg^{2+} into protoporphyrin IX (to form Mg-Proto IX) as the first step of the pathway (Papenbrock et al., 2000). The expression of the Mg-chelatase gene (*MgCHLI1)* was not lower than the samples on potting soil at 7 days, as well as after the cut and, quite unexpectedly, it was significantly higher in PGM leaves at 14 days (Supplementary Fig. 3). Mg-Proto IX was proposed to control the plastid-to-nucleus signal and repress the expression of nuclear genes coding for chloroplastic proteins associated with photosynthesis in conditions when plastid development is impaired (Strand et al., 2003). Later, it was demonstrated that the steady-state level of Mg-Proto IX did not correlate with the expression of photosynthetic genes (Mochizuki et al., 2008). In the experimental set-up here used, PGM experience non-optimal conditions which impact the proper development of leaves and roots; hence, it is expected that a pathway controlling the expression of photosynthetic genes exists in PGM leaves. The levels of Mg-Proto IX were here not measured, but a role of tetrapyrrole signaling pathway in plants in modulating the response to abiotic stresses has been proven (reviewed by Larkin, 2016) and it may be involved in the response of plants to growth on MMS-1.

Sucrose synthase (SuSy) is an important enzyme which provides the nucleotide sugar UDP-glucose necessary for cellulose/callose biosynthesis (Stein and Granot, 2019). The *SuSy* genes investigated showed different behaviour at the different time-points: while *SuSy4* was expressed at higher levels in PGS leaves, *SuSy1* and *SuSy6* were up-regulated in PGM (Supplementary Fig. 3). Taking into account the fundamental role of SuSy in plant development and response to the environment, this result is not unexpected and can be interpreted by considering the multigenic feature of this class of glycosyltransferases. The reduced expression of *SuSy4* in PGM leaves can be explained by the slower growth on MMS-1. *SuSy1* and *SuSy6* expression patterns suggest instead a response to a stressful condition, such as the one caused by the growth on MMS-1.

Among the phenylpropanoid pathway-related genes, *CAD1* was up-regulated in PGM leaves at 7 and 14 days and *PAL1-5* showed statistically significant higher expression in PGM samples at 14 days (Supplementary Fig. 3). An increased thickening of the epidermal cells in PGM leaves could be observed at the level of the cuticle (Fig. 2D) which stained red after FASGA coloration, indicating the presence of lignin/phenolic compounds. The deposition of lignin in PGM leaves can be linked to the mechanism put in place by the plants to avoid water loss; lignin deposition is known to change in response to abiotic stresses (Moura et al., 2010).

The proteomic landscape of PGM roots shows extensive down-regulation of proteins involved in primary metabolism and translation (Table 2): among the proteins showing total repression in PGM roots there are an aldo-keto reductase with similarity to diketogluconate reductase, the ATP synthase protein MI25, structural ribosomal proteins (L18e/L15P eL6, uL5, S6 and eL22), a cytochrome *c*, the stress-responsive protein WRAB, a heat shock protein 90. The response of PGM roots thus involves primarily a decreased protein synthesis, which is triggered by the nutrient deficiency condition experienced by *L. multiflorum*. Primary metabolic pathways (glycolysis, Krebs cycle, lipid metabolism) are down-regulated with consequences on the overall development of the plants. Under nutrient deficiency (especially N), the metabolism slows down and a marked reduction of organic acids of the Krebs cycle was reported in maize (Ganie et al., 2020). Among the down-regulated proteins, the abundance of 3-ketoacyl-CoA synthase decreased >30 fold in PGM roots: this result merged with the data obtained with microscopy is quite indicative of the mechanisms put in place by *L. multiflorum* when growing on MMS-1. In maize, a shortage of N was shown to promote aerenchyma formation via an increased sensitivity to ethylene (Drew et al., 2000) and in some rice varieties aerenchyma occurred in response to ethylene (Justin and Armstrong, 1991). Ethylene, in its turn, interferes with suberin deposition (Barberon et al., 2016). In *L. mutiflorum* roots, the nutrient deficiency of MMS-1 (mainly N) can trigger ethylene-promoted aerenchyma formation and down-regulation of suberin biosynthesis. To verify this hypothesis, however, the levels of ethylene will have to be measured in PGM roots in the future.

In PGM roots, a serine hydroxymethyltransferase together with an adenosylhomocysteinase-AHCY showed a FC PGM vs PGS roots > 7 (Table 2). In PGM roots, the increased abundance of AHCY facilitates the regeneration *S*-adenosyl-methionine (SAM) by removing *S*-adenosyl-homocysteine which is a strong inhibitor of SAM-dependent methyltransferases (Rahikainen et al., 2018). Methylation in plants is an important mechanism for genomic stability via the epigenetic regulation of transposable elements (TEs): DNA methylation is indeed commonly involved in the inactivation of TEs (Ramakrishnan et al., 2021). In support of this methylation-driven TEs silencing mechanism in PGM roots is the 2-fold increased abundance of a SET domain-containing protein involved in histone methylation (Table 2 and Supplementary File 3). The growth on MMS-1 causes an important nutritional and alkaline stress in plants with important consequences on the correct development of the roots and leaves. Under stressful conditions, plants are known to activate TEs silencing via histone methylation and small RNA-directed DNA methylation: this mechanism requires the synthesis of 24 nt-siRNAs by RNA polymerase IV (Pol IV) which in their turn induce *de novo* cytosine methylation in DNA regions showing complementarity to the siRNAs (Saze et al., 2012). Methylation is therefore important as a mechanism of response to exogenous stressors.

In PGS leaves, a strong up-regulation was observed for proteins involved in primary metabolism (glycolysis) and translation (Table 3 and Supplementary File 3). As discussed above for the roots, these results were expected for plants growing on a N- and P-poor substrate such as MMS-1 and considering the chlorotic phenotype observed in the leaf lamina (Fig. 1C).

The existence of a DNA methylation mechanism in plants growing on MMS-1 was supported by the increased abundance of an AHCY, a serine hydroxymethyltransferase and a protein similar to class I-like SAM-binding methyltransferase in PGM leaves (Table 3 and Supplementary File 3).

5. Conclusions

The present investigation provides data concerning the impact on plant growth and development of a simulant reproducing the compositional characteristics of the real Martian regolith. The presence of perchlorate in the real Martian soil, as well as partial gravity will need to be taken into account in future studies focused on space farming. By using *L. multiflorum* as a model of fast-growing herbaceous species, the results here obtained provide evidence on the major phenotypes observed in roots and leaves of plants growing on MMS-1. This study provides information that will be useful to optimise ISRU for long-term space missions. *L. multiflorum* plants were able to grow on MMS-1, even after performing a cut and to produce biomass. This biomass could be used in future space farming systems as source of organic matter to enrich Martian regoliths and thus facilitate the growth and development of further cultivations. Future studies should be directed towards the study of the DNA methylome of plants growing on MMS-1 and of the underlying mechanisms of epigenetic modifications to devise strategies improving crop productivity in a hostile environment. Likewise, future efforts should be focused on understanding how plants can modify the physico-chemical properties of Martian regolith simulants like pH and nutrient availability. Root-based processes relying on the secretion of organic compounds/polysaccharides may be involved and employed using biotechnology to condition Martian regoliths and prepare this growth substrate for the cultivation of crops.

Supplementary data to this article can be found online at https://doi.org/10.1016/j.scitotenv.2022.158774.

CRediT authorship contribution statement

Roberto Berni: Conceptualization, Methodology, Formal analysis, Investigation, Validation, Data curation, Writing – original draft. **Céline C. Leclercq:** Formal analysis, Data curation, Investigation, Writing – review & editing. **Philippe Roux** Investigation, Writing – review & editing. **Jean-Francois Hausman:** Project administration, Writing – review &

editing. **Jenny Renaut:** Methodology, Project administration, Writing – review & editing. **Gea Guerriero:** Conceptualization, Methodology, Supervision, Project administration, Writing – original draft.

Data availability

The data generated are included in the submission or made available through a repository

Declaration of competing interest

The authors declare that they have no known competing financial interests or personal relationships that could have appeared to influence the work reported in this paper.

Acknowledgements

The authors thank Dr. Jean-Thomas Cornélis for the pre-submission review and the insightful comments.

Funding

This research did not receive any specific grant from funding agencies in the public, commercial, or not-for-profit sector.

References

Akisheva, Y., Gourinat, Y., 2021. Utilisation of moon regolith for radiation protection and thermal insulation in permanent lunar habitats. Appl. Sci. 11, 3853. https://doi.org/10.3390/app11093853.

Allen, C.C., Morris, R.V., Jager, K.M., Golden, D.C., Lindstrom, D.J., Lindstrom, M.M., Lockwood, J.P., 1998. Martian Regolith Simulant JSC Mars-1 1690.

Barberon, M., Vermeer, J.E.M., De Bellis, D., Wang, P., Naseer, S., Andersen, T.G., Humbel, B.M., Nawrath, C., Takano, J., Salt, D.E., Geldner, N., 2016. Adaptation of root function by nutrient-induced plasticity of endodermal differentiation. Cell 164, 447–459. https://doi.org/10.1016/j.cell.2015.12.021.

Berliner, A.J., Hilzinger, J.M., Abel, A.J., McNulty, M.J., Makrygiorgos, G., Averesch, N.J.H., Sen Gupta, S., Benvenuti, A., Caddell, D.F., Cestellos-Blanco, S., Doloman, A., Friedline, S., Ho, D., Gu, W., Hill, A., Kusuma, P., Lipsky, I., Mirkovic, M., Luis Meraz, J., Pane, V., Sander, K.B., Shi, F., Skerker, J.M., Styer, A., Valgardson, K., Wetmore, K., Woo, S.-G., Xiong, Y., Yates, K., Zhang, C., Zhen, S., Bugbee, B., Clark, D.S., Coleman-Derr, D., Mesbah, A., Nandi, S., Waymouth, R.M., Yang, P., Criddle, C.S., McDonald, K.A., Seefeldt, L.C., Menezes, A.A., Arkin, A.P., 2021. Towards a biomanufactory on Mars. Front. Astron. Space Sci. 8, 711550. https://doi.org/10.3389/fspas.2021.711550.

Berni, R., Charton, S., Planchon, S., Legay, S., Romi, M., Cantini, C., Cai, G., Hausman, J.-F., Renaut, J., Guerriero, G., 2021. Molecular investigation of tuscan sweet cherries sampled over three years: gene expression analysis coupled to metabolomics and proteomics. Hortic. Res. 8, 12. https://doi.org/10.1038/s41438-020-00445-3.

Bradford, M.M., 1976. A rapid and sensitive method for the quantitation of microgram quantities of protein utilizing the principle of protein-dye binding. Anal. Biochem. 72, 248–254. https://doi.org/10.1006/abio.1976.9999.

Cannon, K.M., Britt, D.T., Smith, T.M., Fritsche, R.F., Batcheldor, D., 2019. Mars global simulant MGS-1: a rocknest-based open standard for basaltic martian regolith simulants. Icarus 317, 470–478. https://doi.org/10.1016/j.icarus.2018.08.019.

Caporale, A.G., Vingiani, S., Palladino, M., El-Nakhel, C., Duri, L.G., Pannico, A., Rouphael, Y., De Pascale, S., Adamo, P., 2020. Geo-mineralogical characterisation of Mars simulant MMS-1 and appraisal of substrate physico-chemical properties and crop performance obtained with variable green compost amendment rates. Sci. Total Environ. 720, 137543. https://doi.org/10.1016/j.scitotenv.2020.137543.

Chen, T.-W., Gan, R.-C., Fang, Y.-K., Chien, K.-Y., Liao, W.-C., Chen, C.-C., Wu, T.H., Chang, I.Y.-F., Yang, C., Huang, P.-J., Yeh, Y.-M., Chiu, C.-H., Huang, T.-W., Tang, P., 2017. FunctionAnnotator, a versatile and efficient web tool for non-model organism annotation. Sci. Rep. 7, 10430. https://doi.org/10.1038/s41598-017-10952-4.

Curie, C., Panaviene, Z., Loulergue, C., Dellaporta, S.L., Briat, J.-F., Walker, E.L., 2001. Maize yellow stripe1 encodes a membrane protein directly involved in Fe(III) uptake. Nature 409, 346–349. https://doi.org/10.1038/35053080.

Curie, C., Cassin, G., Couch, D., Divol, F., Higuchi, K., Le Jean, M., Misson, J., Schikora, A., Czernic, P., Mari, S., 2009. Metal movement within the plant: contribution of nicotianamine and yellow stripe 1-like transporters. Ann. Bot. 103, 1–11. https://doi.org/10.1093/aob/mcn207.

Dai, J., Wang, N., Xiong, H., Qiu, W., Nakanishi, H., Kobayashi, T., Nishizawa, N.K., Zuo, Y., 2018. The yellow stripe-like (YSL) gene functions in internal copper transport in peanut. Genes 9, 635. https://doi.org/10.3390/genes9120635.

De Micco, V., Aronne, G., Colla, G., Fortezza, R., De Pascale, S., 2009. Agro-biology for bioregenerative life support systems in long-term space missions: general constraints and the Italian efforts. J. Plant Interact. 4, 241–252. https://doi.org/10.1080/17429140903161348.

Drew, M.C., He, C.-J., Morgan, P.W., 2000. Programmed cell death and aerenchyma formation in roots. Trends Plant Sci. 5, 123–127. https://doi.org/10.1016/S1360-1385(00)01570-3.

Duri, L.G., El-Nakhel, C., Caporale, A.G., Ciriello, M., Graziani, G., Pannico, A., Palladino, M., Ritieni, A., De Pascale, S., Vingiani, S., Adamo, P., Rouphael, Y., 2020. Mars regolith simulant ameliorated by compost as *in situ* cultivation substrate improves lettuce growth and nutritional aspects. Plants 9, 628. https://doi.org/10.3390/plants9050628.

Duri, L.G., Caporale, A.G., Rouphael, Y., Vingiani, S., Palladino, M., De Pascale, S., Adamo, P., 2022. The potential for lunar and martian regolith simulants to sustain plant growth: a multidisciplinary overview. Front. Astron. Space Sci. 8, 1–16. https://doi.org/10.3389/fspas.2021.747821.

Eisen, M.B., Spellman, P.T., Brown, P.O., Botstein, D., 1998. Cluster analysis and display of genome-wide expression patterns. Proc. Natl. Acad. Sci. U. S. A. 95, 14863–14868.

Ganie, A.H., Pandey, R., Kumar, M.N., Chinnusamy, V., Iqbal, M., Ahmad, A., 2020. Metabolite profiling and network analysis reveal coordinated changes in low-N tolerant and low-N sensitive maize genotypes under nitrogen deficiency and restoration conditions. Plants 9, 1459. https://doi.org/10.3390/plants9111459.

Gao, R., Curtis, T.Y., Powers, S.J., Xu, H., Huang, J., Halford, N.G., 2016. Food safety: structure and expression of the asparagine synthetase gene family of wheat. J. Cereal Sci. 68, 122–131. https://doi.org/10.1016/j.jcs.2016.01.010.

Green, L.S., Rogers, E.E., 2004. FRD3 controls iron localization in arabidopsis. Plant Physiol. 136, 2523–2531. https://doi.org/10.1104/pp.104.045633.

Grotzinger, J.P., Crisp, J., Vasavada, A.R., Anderson, R.C., Baker, C.J., Barry, R., Blake, D.F., Conrad, P., Edgett, K.S., Ferdowski, B., Gellert, R., Gilbert, J.B., Golombek, M., Gómez-Elvira, J., Hassler, D.M., Jandura, L., Litvak, M., Mahaffy, P., Maki, J., Meyer, M., Malin, M.C., Mitrofanov, I., Simmonds, J.J., Vaniman, D., Welch, R.V., Wiens, R.C., 2012. Mars science laboratory mission and science investigation. Space Sci. Rev. 170, 5–56. https://doi.org/10.1007/s11214-012-9892-2.

Guerriero, G., Behr, M., Hausman, J.-F., Legay, S., 2017. Textile hemp vs. Salinity: insights from a targeted gene expression analysis. Genes (Basel) 8. https://doi.org/10.3390/genes8100242.

Guerriero, G., Achen, C., Xu, X., Planchon, S., Leclercq, C.C., Sergeant, K., Berni, R., Hausman, J.-F., Renaut, J., Legay, S., 2021. The cell wall proteome of Craterostigma plantagineum cell cultures habituated to dichlobenil and isoxaben. Cells 10, 2295. https://doi.org/10.3390/cells10092295.

Hu, B., Henry, A., Brown, K.M., Lynch, J.P., 2014. Root cortical aerenchyma inhibits radial nutrient transport in maize (Zea mays). Ann. Bot. 113, 181–189. https://doi.org/10.1093/aob/mct259.

Hu, Z., Zhang, Y., He, Y., Cao, Q., Zhang, T., Lou, L., Cai, Q., 2020. Full-length transcriptome assembly of italian ryegrass root integrated with RNA-seq to identify genes in response to plant cadmium stress. Int. J. Mol. Sci. 21, 1067. https://doi.org/10.3390/ijms21031067.

Hufenbach, B., Laurini, K., Piedboef, J.-C., Schade, B., Matsumoto, K., Spiero, F., Lorenzoni, A., 2011. The global exploration roadmap. IAC-11-B3.1.8, 62nd International Astronautical Congress, Capetown, SA 2011.

Hui, H., Peslier, A.H., Zhang, Y., Neal, C.R., 2013. Water in lunar anorthosites and evidence for a wet early moon. Nat. Geosci. 6, 177–180. https://doi.org/10.1038/ngeo1735.

Justin, S.H.F.W., Armstrong, W., 1991. Evidence for the involvement of ethene in aerenchyma formation in adventitious roots of rice (Oryza sativa L.). New Phytol. 118, 49–62. https://doi.org/10.1111/j.1469-8137.1991.tb00564.x.

Kadioglu, A., Terzi, R., Saruhan, N., Saglam, A., 2012. Current advances in the investigation of leaf rolling caused by biotic and abiotic stress factors. Plant Sci. 182, 42–48. https://doi.org/10.1016/j.plantsci.2011.01.013.

Karl, D., Kamutzki, F., Lima, P., Gili, A., Duminy, T., Zocca, A., Günster, J., Gurlo, A., 2020. Sintering of ceramics for clay *in situ* resource utilization on Mars. Open Ceram. 3, 100008. https://doi.org/10.1016/j.oceram.2020.100008.

Kasiviswanathan, P., Swanner, E.D., Halverson, L.J., Vijayapalani, P., 2022. Farming on Mars: treatment of basaltic regolith soil and briny water simulants sustains plant growth. PLoS ONE 17, e0272209. https://doi.org/10.1371/journal.pone.0272209.

Larkin, R.M., 2016. Tetrapyrrole signaling in plants. Front. Plant Sci. 7 (7), 1586. https://doi.org/10.3389/fpls.2016.01586.

Lasseur, C., Brunet, J., Weever, H.de, Dixon, M., Dussap, G., Godia, F., Leys, N., Mergeay, M., Straeten, D.V.D., 2010. MELiSSA: the European project of closed life support system. Gravit. Space Res. 23.

Lea, P.J., Sodek, L., Parry, M.A.J., Shewry, P.R., Halford, N.G., 2007. Asparagine in plants. Ann. Appl. Biol. 150, 1–26.

Li, Q., Chen, L., Yang, A., 2019. The molecular mechanisms underlying iron deficiency responses in rice. Int. J. Mol. Sci. 21, 43. https://doi.org/10.3390/ijms21010043.

Liu, J., Wang, Y., Li, Q., 2017. Analysis of differentially expressed genes and adaptive mechanisms of Prunus triloba lindl. Under alkaline stress. Hereditas 154, 10. https://doi.org/10.1186/s41065-017-0031-7.

Llorente, B., Williams, T.C., Goold, H.D., 2018. The multiplanetary future of plant synthetic biology. Genes 9, 348. https://doi.org/10.3390/genes9070348.

Menezes, A.A., Montague, M.G., Cumbers, J., Hogan, J.A., Arkin, A.P., 2015. Grand challenges in space synthetic biology. J. R. Soc. Interface 12, 20150803. https://doi.org/10.1098/rsif.2015.0803.

Metsalu, T., Vilo, J., 2015. ClustVis: a web tool for visualizing clustering of multivariate data using principal component analysis and heatmap. Nucleic Acids Res. 43, W566–W570. https://doi.org/10.1093/nar/gkv468.

Meurisse, A., Carpenter, J., 2020. Past, present and future rationale for space resource utilisation. Planet. Space Sci. 182, 104853. https://doi.org/10.1016/j.pss.2020.104853.

Mochizuki, N., Tanaka, R., Tanaka, A., Masuda, T., Nagatani, A., 2008. The steady-state level of mg-protoporphyrin IX is not a determinant of plastid-to-nucleus signaling in arabidopsis. PNAS 105, 15184–15189. https://doi.org/10.1073/pnas.0803245105.

Möhlmann, D.T.F., 2004. Water in the upper martian surface at mid- and low-latitudes: presence, state, and consequences. Icarus 168, 318–323. https://doi.org/10.1016/j.icarus.2003.11.008.

Moura, J.C.M.S., Bonine, C.A.V., Viana, J.D.O.F., Dornelas, M.C., Mazzafera, P., 2010. Abiotic and biotic stresses and changes in the lignin content and composition in plants. J. Integr. Plant Biol. 52, 360–376. https://doi.org/10.1111/j.1744-7909.2010.00892.x.

Nardi, S., Concheri, G., Pizzeghello, D., Sturaro, A., Rella, R., Parvoli, G., 2000. Soil organic matter mobilization by root exudates. Chemosphere 41, 653–658. https://doi.org/10.1016/s0045-6535(99)00488-9.

Ni, X.-L., Gui, M.-Y., Tan, L.-L., Zhu, Q., Liu, W.-Z., Li, C.-X., 2019. Programmed cell death and aerenchyma formation in water-logged sunflower stems and its promotion by ethylene and ROS. Front. Plant Sci. 9, 1928. https://doi.org/10.3389/fpls.2018.01928.

Oddy, J., Raffan, S., Wilkinson, M.D., Elmore, J.S., Halford, N.G., 2020. Stress, nutrients and genotype: understanding and managing asparagine accumulation in wheat grain. CABI Agric. Biosci. 1, 10. https://doi.org/10.1186/s43170-020-00010-x.

Ouyang, W., Yin, X., Yang, J., Struik, P.C., 2020. Comparisons with wheat reveal root anatomical and histochemical constraints of rice under water-deficit stress. Plant Soil 452, 547–568. https://doi.org/10.1007/s11104-020-04581-6.

Oze, C., Beisel, J., Dabsys, E., Dall, J., North, G., Scott, A., Lopez, A.M., Holmes, R., Fendorf, S., 2021. Perchlorate and agriculture on Mars. Soil Systems 5, 37. https://doi.org/10.3390/soilsystems5030037.

Pan, L., Zhang, X., Wang, J., Ma, X., Zhou, M., Huang, L., Nie, G., Wang, P., Yang, Z., Li, J., 2016. Transcriptional profiles of drought-related genes in modulating metabolic processes and antioxidant defenses in Lolium multiflorum. Front. Plant Sci. 7, 519. https://doi.org/10.3389/fpls.2016.00519.

Papenbrock, J., Mock, H.-P., Tanaka, R., Kruse, E., Grimm, B., 2000. Role of magnesium chelatase activity in the early steps of the tetrapyrrole biosynthetic pathway. Plant Physiol. 122, 1161–1170.

Paul, A.-L., Elardo, S.M., Ferl, R., 2022. Plants grown in apollo lunar regolith present stress-associated transcriptomes that inform prospects for lunar exploration. Commun. Biol. 5, 1–9. https://doi.org/10.1038/s42003-022-03334-8.

Peters, G.H., Abbey, W., Bearman, G.H., Mungas, G.S., Smith, J.A., Anderson, R.C., Douglas, S., Beegle, L.W., 2008. Mojave Mars simulant—characterization of a new geologic Mars analog. Icarus 197, 470–479. https://doi.org/10.1016/j.icarus.2008.05.004.

Pétriacq, P., Williams, A., Cotton, A., McFarlane, A.E., Rolfe, S.A., Ton, J., 2017. Metabolite profiling of non-sterile rhizosphere soil. Plant J. 92, 147–162. https://doi.org/10.1111/tpj.13639.

Pickett, M.T., Roberson, L.B., Calabria, J.L., Bullard, T.J., Turner, G., Yeh, D.H., 2020. Regenerative water purification for space applications: needs, challenges, and technologies towards "closing the loop". Life Sci. Space Res. 24, 64–82. https://doi.org/10.1016/j.lssr.2019.10.002.

Postma, J.A., Lynch, J.P., 2011. Root cortical aerenchyma enhances the growth of maize on soils with suboptimal availability of nitrogen, phosphorus, and potassium. Plant Physiol. 156, 1190–1201. https://doi.org/10.1104/pp.111.175489.

Qian, Y., Xiao, L., Head, J.W., van der Bogert, C.H., Hiesinger, H., Wilson, L., 2021. Young lunar mare basalts in the Chang'e-5 sample return region, northern Oceanus procellarum. Earth Planet. Sci. Lett. 555, 116702. https://doi.org/10.1016/j.epsl.2020.116702.

Rahikainen, M., Alegre, S., Trotta, A., Pascual, J., Kangasjärvi, S., 2018. Trans-methylation reactions in plants: focus on the activated methyl cycle. Physiol. Plant. 162, 162–176. https://doi.org/10.1111/ppl.12619.

Ramakrishnan, M., Satish, L., Kalendar, R., Narayanan, M., Kandasamy, S., Sharma, A., Emamverdian, A., Wei, Q., Zhou, M., 2021. The dynamism of transposon methylation for plant development and stress adaptation. Int. J. Mol. Sci. 22, 11387. https://doi.org/10.3390/ijms222111387.

Ramkissoon, N.K., Pearson, V.K., Schwenzer, S.P., Schröder, C., Kirnbauer, T., Wood, D., Seidel, R.G.W., Miller, M.A., Olsson-Francis, K., 2019. New simulants for martian regolith: controlling iron variability. Planet. Space Sci. 179, 104722. https://doi.org/10.1016/j.pss.2019.104722.

Rodriguez-Celma, J., Pan, I.-C., Li, W., Lan, P., Buckhout, T., Schmidt, W., 2013. The transcriptional response of Arabidopsis leaves to Fe deficiency. Front. Plant Sci. 4, 276. https://doi.org/10.3389/fpls.2013.00276.

Römheld, V., 1991. The role of phytosiderophores in acquisition of iron and other micronutrients in graminaceous species: an ecological approach. Plant Soil 130, 127–134. https://doi.org/10.1007/BF00011867.

Rubio, V., Linhares, F., Solano, R., Martín, A.C., Iglesias, J., Leyva, A., Paz-Ares, J., 2001. A conserved MYB transcription factor involved in phosphate starvation signaling both in vascular plants and in unicellular algae. Genes Dev. 15, 2122–2133. https://doi.org/10.1101/gad.204401.

Saengwilai, P., Nord, E.A., Chimungu, J.G., Brown, K.M., Lynch, J.P., 2014. Root cortical aerenchyma enhances nitrogen acquisition from low-nitrogen soils in maize. Plant Physiol. 166, 726–735. https://doi.org/10.1104/pp.114.241711.

Saldanha, A.J., 2004. Java Treeview–extensible visualization of microarray data. Bioinformatics 20, 3246–3248. https://doi.org/10.1093/bioinformatics/bth349.

Salisbury, F.B., 1999. Growing crops for space explorers on the moon, Mars, or in space. Adv. Space Biol. Med. 7, 131–162. https://doi.org/10.1016/s1569-2574(08)60009-x.

Santos, C.S., Ozgur, R., Uzilday, B., Turkan, I., Roriz, M., Rangel, A.O.S.S., Carvalho, S.M.P., Vasconcelos, M.W., 2019. Understanding the role of the antioxidant system and the tetrapyrrole cycle in iron deficiency chlorosis. Plants (Basel) 8, 348. https://doi.org/10.3390/plants8090348.

Saze, H., Tsugane, K., Kanno, T., Nishimura, T., 2012. DNA methylation in plants: relationship to small RNAs and histone modifications, and functions in transposon inactivation. Plant Cell Physiol. 53, 766–784. https://doi.org/10.1093/pcp/pcs008.

Schleppi, J., Gibbons, J., Groetsch, A., Buckman, J., Cowley, A., Bennett, N., 2019. Manufacture of glass and mirrors from lunar regolith simulant. J. Mater. Sci. 54, 3726–3747. https://doi.org/10.1007/s10853-018-3101-y.

Sega, P., Pacak, A., 2019. Plant PHR transcription factors: put on a map. Genes (Basel) 10, 1018. https://doi.org/10.3390/genes10121018.

Stein, O., Granot, D., 2019. An overview of sucrose synthases in plants. Front. Plant Sci. 10, 95. https://doi.org/10.3389/fpls.2019.00095.

Strand, A., Asami, T., Alonso, J., Ecker, J.R., Chory, J., 2003. Chloroplast to nucleus communication triggered by accumulation of mg-protoporphyrinIX. Nature 421, 79–83. https://doi.org/10.1038/nature01204.

Tolivia, D., Tolivia, J., 1987. Fasga: a new polychromatic method for simultaneous and differential staining of plant tissues. J. Microsc. 148, 113–117. https://doi.org/10.1111/j.1365-2818.1987.tb02859.x.

Vandesompele, J., De Preter, K., Pattyn, F., Poppe, B., Van Roy, N., De Paepe, A., Speleman, F., 2002. Accurate normalization of real-time quantitative RT-PCR data by geometric averaging of multiple internal control genes. Genome Biol. 3, 1 research0034.

Villacampa, A., Ciska, M., Manzano, A., Vandenbrink, J.P., Kiss, J.Z., Herranz, R., Medina, F.J., 2021. From spaceflight to Mars g-levels: adaptive response of a. Thaliana seedlings in a reduced gravity environment is enhanced by red-light photostimulation. Int. J. Mol. Sci. 22, 899. https://doi.org/10.3390/ijms22020899.

Vizcaíno, J.A., Csordas, A., del-Toro, N., Dianes, J.A., Griss, J., Lavidas, I., Mayer, G., Perez-Riverol, Y., Reisinger, F., Ternent, T., Xu, Q.-W., Wang, R., Hermjakob, H., 2016. 2016 update of the PRIDE database and its related tools. Nucleic Acids Res 44, D447–D456. https://doi.org/10.1093/nar/gkv1145.

Wamelink, G.W.W., Frissel, J.Y., Krijnen, W.H.J., Verwoert, M.R., Goedhart, P.W., 2014. Can plants grow on Mars and the moon: a growth experiment on Mars and moon soil simulants. PLoS ONE 9, e103138. https://doi.org/10.1371/journal.pone.0103138.

Wamelink, G.W.W., Frissel, J.Y., Krijnen, W.H.J., Verwoert, M.R., 2019. Crop growth and viability of seeds on Mars and moon soil simulants. Open Agric. 4, 509–516. https://doi.org/10.1515/opag-2019-0051.

Waters, B.M., McInturf, S.A., Stein, R.J., 2012. Rosette iron deficiency transcript and microRNA profiling reveals links between copper and iron homeostasis in Arabidopsis thaliana. J. Exp. Bot. 63, 5903–5918. https://doi.org/10.1093/jxb/ers239.

Xu, X., Legay, S., Sergeant, K., Zorzan, S., Leclercq, C.C., Charton, S., Giarola, V., Liu, X., Challabathula, D., Renaut, J., Hausman, J.-F., Bartels, D., Guerriero, G., 2021. Molecular insights into plant desiccation tolerance: transcriptomics, proteomics and targeted metabolite profiling in Craterostigma plantagineum. Plant J. 107, 377–398. https://doi.org/10.1111/tpj.15294.

Zakari, S.A., Asad, M.-A.-U., Han, Z., Zhao, Q., Cheng, F., 2020. Relationship of nitrogen deficiency-induced leaf senescence with ROS generation and ABA concentration in rice flag leaves. J. Plant Growth Regul. 39, 1503–1517. https://doi.org/10.1007/s00344-020-10128-x.

Zhang, C., Shinwari, K.I., Luo, L., Zheng, L., 2018. OsYSL13 is involved in iron distribution in rice. Int. J. Mol. Sci. 19, 3537. https://doi.org/10.3390/ijms19113537.

Zhang, T., Xu, K., Yao, Z., Ding, X., Zhao, Z., Hou, X., Pang, Y., Lai, X., Zhang, W., Liu, S., Deng, J., 2019. The progress of extraterrestrial regolith-sampling robots. Nat. Astron. 3, 487–497. https://doi.org/10.1038/s41550-019-0804-1.

Zheng, L., Yamaji, N., Yokosho, K., Ma, J.F., 2012. YSL16 is a phloem-localized transporter of the copper-nicotianamine complex that is responsible for copper distribution in rice. Plant Cell 24, 3767–3782. https://doi.org/10.1105/tpc.112.103820.